5-2007

Design Optimization of Flattop Interleaver and Its Dispersion Compensation

Li Wei
Wilfrid Laurier University, lwei@wlu.ca

John W.Y. Lit
Wilfrid Laurier University, jlit@wlu.ca

Design optimization of flattop interleaver and its dispersion compensation

L. Wei and J. W. Y. Lit

Department of Physics and Computer Science, Wilfrid Laurier University, Waterloo, N2L 3C5, Canada
lwei@wlu.ca

Abstract: The objective of this paper is to present a general strategy for design optimization of flattop interleavers, and dispersion compensation for the interleavers, in order to achieve superior optical performance. The interleaver is formed by two multi-cavity Gire-Tournois etalons (MC-GTE) in a Michelson Interferometer (MI). An interleaver that has *m* cavities in one etalon and *n* cavities in the other is called an *mn*-GTE interleaver. Our optimization strategy exploits the general flattop condition and the technique of ripple equalization. Any *mn*-GTE interleaver may be optimized. The spectral performance can be greatly improved by the optimization process. As an illustration, we present a comprehensive analysis for a 11-GTE and a 21-GTE interleaver. The analytical expressions for flattop conditions, peak and trough positions are derived for optimization. The optimal performance of the interleavers can be controlled by the reflection coefficients and the parameters *m* and *n*. To achieve low-dispersion *mn*-GTE flattop interleavers, we propose to use one additional MC-GTE as a dispersion compensator to compensate for the chromatic dispersion. The analytical expressions of group delays and chromatic dispersions for an MC-GTE interleaver are derived. The optimization strategy of dispersion-ripple equalization is explained. The results show that the dispersion performance can be tailored by changing the reflection coefficients of the MC-GTE, and the dispersion and bandwidth can be enhanced by increasing the number of cavities of the MC-GTE.

OCIS codes: (060.2340) Fiber optics components; (060.1810) Couplers, switches, multiplexers; (120.2230) Fabry-Perot; (120.2440) Filters; (350.2460) Filters, interference

References and links

1. S. Cao, J. Chen, J. N. Damask, C. R. Doerr, L. Guiziou, G. Harvey, Y. Hibino, H. Li, S. Suzuki, K. Y. Wu and P. Xie, "Integrated technology: comparisons and applications requirements," J. Lightwave Technol. **22**, 281-289 (2004).
2. K. Jinguji and M. Oguma, "Optical half-band filters," J. Lightwave Technol. **18**, 252-259 (2000).
3. M. Oguma, T. Kitoh, Y. Inoue, T. Mizuno, T. Shibata, M. Kohtoku and Y. Hibino, "Compact and low-loss interleaver filter employing lattice-form structure and silica-based waveguide," J. Lightwave Technol. **22**, 895-902 (2004).
4. C. H. Huang, Y. Li, J. Chen, E. Sidick, J. Chon, K. G. Sullivan, and J. Bautista, "Loss-loss flat-top 50-GHz DWDM and Add/Drop modules using all-fiber Fourier filters," NFOEC, 311-316 (2000).
5. Q. J. Wang, T. Liu and Y. C. Soh, "All-fiber Fourier filter flat-top interleaver design with specified performance parameters," Opt. Eng. **42**, 3172-3178 (2003).
6. J. Zhang and L. Liu, "Novel Mach-Zehnder interferometer structure for tunable optical interleaver," Opt. Eng. **45**, 045003 (2006).
7. Y. Lai, W. Zhang, J. A. R. Williams and I. Bennion, "Bidirectional nonreciprocal wavelength-interleaving coherent fiber transversal filter," IEEE Photon. Technol. Lett. **16**, 500–502 (2004).
8. Y. W. Lee, H. Kim, J. Jung and B. Lee, "Wavelength-switchable flat-top fiber comb filter based on a Solc type birefringence combination," Opt. Express. **13**, 1039-1048 (2005).
9. H. F. Taylor, "Design of multireflector resonant bandpass filters for guided wave optics," J. Lightwave Technol. **19**, 866-871 (2001).

#79720 - $15.00 USD Received 5 Feb 2007; revised 10 Apr 2007; accepted 17 Apr 2007; published 11 May 2007

10. L. P. Ghislain, R. Sommer, R. J. Ryall, R. M. Fortenberry, D. Derickson, P. C. Egerton, M. R. Kozlowski, D. J. Poirger, S. DeMange, L. F. Stokes, and M. A. Scobey, "Miniature solid etalon interleaver," NFOEC, 1397-1403 (2001).
11. R. Orta, P. Savi, R. Tascone, and D. Trinchero, "Synthesis of multiple-ring-resonator filters for optical systems," IEEE Photon. Technol. Lett. **7**, 1447-1449 (1995).
12. B. B. Dingel and M. Izutsu, "Multifunction optical filter with a Michelson-Gires-Tournois interferometer for wavelength-division-multiplexed network system applications," Opt. Lett. **23**, 1099-1101 (1998).
13. B. B. Dingel and T. Aruga, "Properties of a novel noncascaed type, easy-to-design, ripple-free optical bandpass filter," J. Lightwave Technol. **17**, 1461-1469 (1999).
14. C. Hsieh, R. Wang, Z. J. Wen, I. McMichael, P. Yeh, C. Lee, and W. Cheng, "Flat-top interleavers using two Gires-Tournois etalons as phase-dispersive mirrors in a Michelson interferometer," IEEE Photon. Technol. Lett. **15**, 242-244 (2003).
15. C. Hsieh, C. W. Lee, S. Y. Huang, R. Wang, P. Yeh and W. H. Cheng, "Flat-top and low-dispersion interleavers using Gires-Tournois etalons as phase dispersive mirrors in a Michelson interferometer," Opt. Commun. **237**, 285-293 (2004).
16. L. Wei and J. W. Y. Lit, "Design of periodic bandpass filters based multi-reflectors Gires-Tournois resonator for WDM systems," Opt. Commun. **255**, 209-217, (2005).
17. S. Cao, C. Lin, C. Yang, E. Ning, J. Zhao, and G. Barbarossa, "Birefrigent Gires-Tournois interferometer (BGTI) for DWDM interleaving," OFC, Anaheim, CA, ThC3 (2002).
18. X. Shu, K. Sugden, and I. Bennion, "Novel multipassband optical filter using all-fiber Michelson-Gires-Tournois Structure," IEEE Photon. Technol. Lett. **17**, 384-386 (2005).
19. Q. J. Wang, Y. Zhang, and Y. C. Soh, "Efficient structure for optical interleavers using superimposed Chirped Fiber Bragg Gratings," IEEE Photon. Technol. Lett. **17**, 387-389 (2005).
20. M. Kohtoku, S. Oku, Y. Kadota, Y. Shibata, and Y. Yoshikuni, "Flattened transmission and rejection band by using a Mach-Zehnder interferometer with a ring resonator," IEEE Photon. Technol. Lett. **12**, 1174-1176 (2000).
21. C. K. Madsen, "Efficient architectures for exactly realizing optical filters with optimum bandpass designs," IEEE Photon. Technol. Lett. **10**, 1136-1138 (1998).
22. Q. J. Wang, Y. Zhang, and Y. C. Soh, "Design of 100/300 GHz optical interleaver with IIR architectures," Opt. Express **13**, 2643-2652 (2005).
23. X. Ye, M. Zhang, and P. Ye, "Flat-top interleavers with chromatic dispersion compensator based on phase dispersive free space Mach-Zehnder interferometer," Opt. Commun. **257**, 255-260 (2006).
24. C. W. Lee, R. Wang, P. Yeh, and W. H. Cheng, "Sagnac interferometer based flat-top birefringent interleaver," Opt. Express **14**, 4636-4643 (2006).
25. G. Lenz and C. K. Madsen, "General optical all-pass filter structures for dispersion control in WDM systems," J. Lightwave Technol. **17**, 1248-1250 (1999).
26. C. J. Kaalund and G. D. Peng, "Pole-zero diagram approach to the design of ring resonator-based fitlers for photonic applications," J. Lightwave Technol. **22**, 1548-1559 (2004).
27. D. J. Moss, M. Lamont, S. McLaughlin, G. Randall, P. Colbourne, S. Kiran, and C. A. Hulse, "Tunable dispersion and dispersion slope compensators for 10 Gb/s using all-pass multicavity etalons," IEEE Photon. Technol. Lett. **15**, 730-732 (2003).
28. L. M. Lunardi, D. J. Moss, S. Chandrasekhar, L. L. Buhl, M. Lamont, S. McLaughlin, G. Randall, P. Colbourne, S. Kiran and C. A. Hulse, "Tunable dispersion compensation at 40-Gb/s using a multicavity etalon all-pass filter with NRZ, RZ, and CS-RZ modulation," J. Lightwave Technol. **20**, 2136-2144 (2002).
29. H. Angus Macleod, *Thin Film Optical Filter*, 2nd edition, (McGraw-Hill Publishing Company, New York, 1989) pp. 51.
30. E. Hecht, *Optics*, 4th edition, (Addison Wesley 2002) pp. 420.

1. Introduction

Dense wavelength-division multiplexing (DWDM) systems are commonly deployed in optical transport systems to increase the system capacities. In DWDM systems with many channels, optical interleavers are widely recognized as an essential component to bridge existing and new DWDM platforms, and to upgrade existing network capacities. Used as a demux (or mux) device, an interleaver can separate a set of periodically spaced wavelengths into two complementary sets – even and odd channels at twice the original spacing (or to combine two sets of even and odd channels into one set of wavelengths at half the original spacing). An interleaver with a 100 GHz free spectral range (FSR) is usually called a 50 GHz Interleaver. The use of interleavers has provided much design flexibility to manage and to route

#79720 - $15.00 USD Received 5 Feb 2007; revised 10 Apr 2007; accepted 17 Apr 2007; published 11 May 2007

wavelengths at any point in a network. Such techniques have been receiving intense attention [1-26] from a large number of research groups all over the world.

An interleaver is basically a periodic *flattop* comb filter. Two types of periodic optical filters, i.e., finite-impulse-response (FIR) filter and infinite-impulse-response (IIR) filter, can be used to make a flattop interleaver. The difference between FIR and IIR filters is that FIR filters have optical feed-forward interference path (without resonance) while IIR filters have optical feed-back interference path (with resonance). A typical example of a FIR filter is a Mach-Zehnder interferometer (MZI), Michelson Interferometer (MI) or Sagnac interferometer (SI), and that of an IIR filter is an etalon or ring resonator (RR). However, in order to realize flattop interleavers, interferometers with two or more stages have to be employed, e.g., cascaded MZI and multi-cavity etalons in FIR and IIR structures, respectively. For example, FIR lattice structures [2-8] using cascaded multi-stage MZI are commonly used to build flattop interleavers with different architectures based on planar waveguides [3], fiber couplers [4-5], optical glass pairs [6], and high birefringence (Hi-Bi) fibers [7-8]; IIR structures using multi-cavity etalon [9-10] or cascaded RR [11] are also commonly used.

Another very attractive approach is based on a combination of feed-forward interference (e.g., MI or MZI or SI) and feed-back interference (e.g., etalon or RR). Such an approach may exploit the advantages of both FIR and IIR filters. Various configurations have been proposed and demonstrated by combining Gires-Tournois etalon (GTE) and MI [12-19], or RR and MZI [20-23], or RR and SI [24]. The GTE–MI structure makes use of GTE to create IIR where GTE replaces one or both fully reflective mirrors, and this structure may be implemented in bulk-optic devices with dielectric thin-film mirrors [14-17] or all-fiber devices with fiber Bragg gratings and a fiber coupler [18-19]. Note that as both GTE and RR are all-pass filters and an MI can be conceptually "unfolded" into an MZI, an analogy to GTE–MI structure is RR–MZI structure. The RR–MZI structure is based on inserting RR (to create IIR) into one or both interference arms, which may be implemented by 2x2 couplers in semiconductor waveguide [20-21], 3x3 fiber couplers [22] or dielectric thin-film mirrors [23]. In the RR–SI structure [24], the feed-forward interference is realized by using polarization interference in an SI. Among these combination structures, GTE based MI has recently attracted much attention. Dingel et al. [12-13] first proposed one single-cavity GTE based MI. Improved designs have been made by Hsieh et al. using two single-cavity GTEs based MI [14-15] and by Wei et al. using one multi-cavity GTE (MC-GTE) based MI [16]. In order to accommodate more and more channels in DWDM systems to further increase the transport system capacities, the specifications of interleavers (e.g., ripple, bandwidth, isolation and dispersion) are becoming more and more tighter. Therefore, developing flattop interleavers with superior performance to meet the current tight specifications is a remaining challenge that has important benefits.

Following our previous work [16], in this paper, we propose to use two MC-GTEs to form an MI for a flattop interleaver, and an additional MC-GTE as a dispersion compensator to achieve superior performance on both spectral response and dispersion. The purpose of this paper is twofold. Firstly, we will present analytical expressions and a general spectral optimization strategy for the double MC-GTE interleaver. The proposed optimization strategy exploits both the flattop conditions and the technique of ripple equalization. We will show how to combine the general flattop conditions and equalization of ripples to achieve spectral optimization for interleavers. Although the general flattop conditions were introduced in ref. [16] for an MI with a single MC-GTE, little has been said about the design optimization, which is obviously much more important for complicated systems such as the present interleaver with two MC-GTEs. Note that an analogy to the present structure would be a coupled multi RR in each arm of an MZI. A similar structure formed by a cascaded multi RR in each arm of an MZI was reported by Madsen [21], and it was analyzed using Z-transform in a digital processing approach. Such an approach was recently widely applied in optical filter designs [19, 21, 25]. Pole-Zero diagram approach [26] was also developed for photonic

#79720 - $15.00 USD Received 5 Feb 2007; revised 10 Apr 2007; accepted 17 Apr 2007; published 11 May 2007

filter design. In contrast, in the present approach we use two-beam interferometry analysis to find the analytical expressions for all physical quantities (such as the intensity, phase, etc.) and the equations that directly optimize the optical performance. Previous works [12-15, 23] that are based on two-beam interferometry analysis only examine physical quantities in single-cavity case.

Secondly, we will present a comprehensive study on chromatic dispersion compensation for the proposed interleaver. Unlike pure FIR-based interleavers, chromatic dispersion is an unavoidable issue for IIR-based interleavers; this has been discussed in ref. [15]. GTEs are commonly employed for tunable constant dispersion compensation [27-28]. However, there is little study on the use of GTEs for the dispersion compensation of IIR-based interleavers. We believe that this paper will provide a complete theoretical foundation and excellent design guidance for researchers in the academic and industry sectors who work on GTE-based optical devices.

The flattop interleaver formed by two MC-GTEs (with any number of cavities) in an MI is presented in Section 2. In Section 2.1, we start with the theory and the formulation for the proposed interleaver. In Section 2.2, we introduce the general method on how to obtain flattop spectrum and how to optimize designs. In Section 3 we present the use of an additional MC-GTE for chromatic dispersion compensation to achieve low-dispersion interleavers. The general theory is given in Section 3.1 and the design optimization is discussed in Section 3.2.

2. Flattop interleaver with two MC-GTEs in an MI

In this section, we present a new approach for optimizing optical spectral performance of the proposed interleaver. To analyse and optimize the optical performance, including the bandwidth, ripple and isolation, the general analytical expressions for the electric fields together with the phases are first derived. Then we introduce our optimization strategy for spectral response, which combines the flattop conditions and the technique of ripple equalization. The general conditions, and the positions of the peaks and the troughs for design optimization are derived, followed by the results and discussions.

2.1 Configuration and formulations for the proposed interleaver

Figure 1 shows the schematic diagram of the proposed interleaver. It is formed by an MI with two MC-GTEs for the two arms of the interferometer. Obviously, MC-GTE is the basic component to build the interleaver. To obtain the general normalized intensities of the interleaver, we first derive the general formulas for an MC-GTE, and then for the interleaver with two MC-GTEs, followed by the special features for the proposed interleavers.

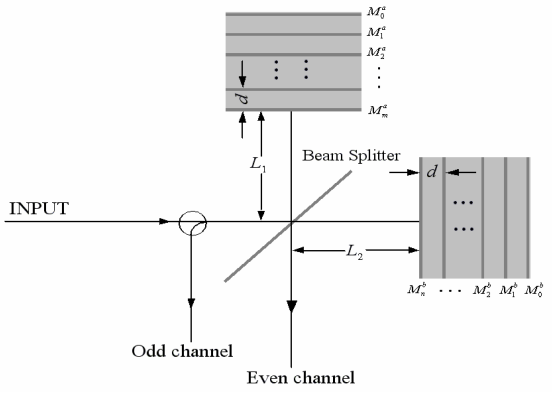

Fig. 1. Schematic diagram of the proposed interleaver

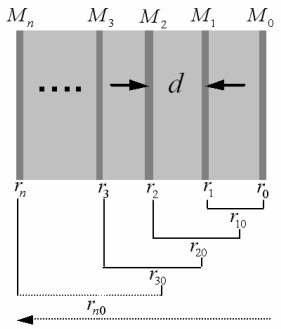

Fig. 2. Schematic diagram of MC-GTE.

#79720 - $15.00 USD Received 5 Feb 2007; revised 10 Apr 2007; accepted 17 Apr 2007; published 11 May 2007

2.1.1 MC-GTE

The MC-GTE consists of N +1 equally spaced reflectors, M_0, M_1, M_2,…, and M_n, as shown in Fig. 2. The reflectances and reflection coefficients of the N +1 reflectors are R_0, R_1, R_2, …, R_n, and r_0, r_1, r_2, …, r_n, respectively, and the cavity length is d. The reflectance R_0 of the rear reflector is assumed to be unity so theoretically the MC-GTE is a lossless all-pass filter, whereas the resultant phase is dispersive, i.e, wavelength dependent. To find the resultant reflection coefficient r of the MC-GTE, we start with the last rear single-cavity etalon formed by M_1 (with r_1) and M_0 (with r_0). The resultant reflection coefficient r_{10} of the last rear single cavity (see Fig. 2) can be written as [29]:

$$r_{10} = \frac{r_1 + r_0 e^{-i2\delta}}{1 + r_1 r_0 e^{-i2\delta}} = -e^{i2\phi_1}, \tag{1}$$

with

$$\phi_1 = -\tan^{-1}(a_1 \tan\delta), \tag{2}$$

where $a_1 = (1+r_1)/(1-r_1)$, and $\delta = 2\pi nd/\lambda$ is the phase shift of each single cavity, n is the refractive index of the cavity, and λ is the wavelength in vacuum.

Next, we study the rear coupled two-cavity etalon (with M_0, M_1, M_2), treating it as a single-cavity etalon formed by M_2 (with r_2) and M_1M_0 (with r_{10}), and find the resultant reflection coefficient r_{20} of the two-cavity etalon. Similarly, we can treat the rear three-cavity etalon (with M_0, M_1, M_2, M_3) as a single-cavity etalon formed by M_3 (with r_3) and $M_2M_1M_0$ (with r_{20}) to find the resultant reflection coefficient r_{30} of the three-cavity etalon, and so on. Finally, by continuing to work toward the left up to reflector M_n, the resultant reflection coefficient r_{n0} for the MC-GTE can be obtained recursively from $r_{(n-1)0}$ (the reflection coefficient of the MC-GTE with N reflectors) as:

$$r_{n0} = \frac{r_n + r_{(n-1)0} e^{-i2\delta}}{1 + r_n r_{(n-1)0} e^{-i2\delta}} = -e^{i2\phi_n}. \tag{3}$$

The resultant phase of the MC-GTE is equal to $2\phi_n$, which can be recursively found from:

$$\phi_n = -\tan^{-1}\left[a_n \tan(\delta - \phi_{n-1})\right], \tag{4}$$

with

$$a_n = (1+r_n)/(1-r_n). \tag{5}$$

2.1.2 Two MC-GTEs in an MI interleaver

As shown in Fig. 1, the proposed interleaver is constructed with two sets of MC-GTEs, a 50:50 beam splitter, and an optical circulator for outputting the odd channels while the even channels exit from the beam splitter. The vertically placed MC-GTE-*a* is an *m*-cavity GTE formed by m +1 equally spaced reflectors – $M_0^a, M_1^a, ..., M_m^a$, and the horizontal-placed MC-GTE-*b* is an *n*-cavity GTE formed by n +1 equally spaced reflectors – $M_0^b, M_1^b, ..., M_n^b$, where the superscripts *a* and *b* are used to distinguish the two MC-GTEs. Accordingly, the reflection coefficients of the MC-GTE-*a* and MC-GTE-*b* are $r_0^a, r_1^a, ..., r_m^a$, and $r_0^b, r_1^b, ..., r_n^b$, respectively. The cavity length is d and the refractive index of the spacer is n for both MC-GTEs. Clearly, the interleaver is a modified MI by replacing two regular 100% mirrors replaced by two sets of MC-GTEs.

In the following, an MI interleaver with two MC-GTEs which have respectively m and n cavities, is called an *mn*-GTE interleaver. For example, a 10-GTE interleaver has a regular reflector (without GTE) in the horizontal arm and a single-cavity GTE in the vertical arm of the interferometer. This is the interleaver in Ref. [12-13]. In another example, a 11-GTE

#79720 - $15.00 USD Received 5 Feb 2007; revised 10 Apr 2007; accepted 17 Apr 2007; published 11 May 2007

interleaver has a single-cavity GTE in each of the interference arms, such as the interleaver in Refs. [14-15].

To analyze the optical performance of the interleaver, we need to find the normalized electrical field and intensity. The electrical field can be written as:

$$E = e^{i(\phi_m+\theta_n)-i\beta(L_1+L_2)}\cos(\triangle\psi-\beta\cdot\triangle L) \tag{6}$$

with

$$\begin{cases} 2\phi_m = -2\tan^{-1}\left[a_m\tan(\delta-\phi_{m-1})\right] \\ 2\theta_n = -2\tan^{-1}\left[b_n\tan(\delta-\theta_{n-1})\right], \end{cases} \tag{7}$$

$$\begin{cases} \triangle\psi = \theta_n-\phi_m \\ \triangle L = L_2-L_1, \end{cases} \tag{8}$$

and

$$\begin{cases} a_m = (1+r_m^a)/(1-r_m^a) \\ b_n = (1+r_n^b)/(1-r_n^b), \end{cases} \tag{9}$$

where $2\phi_m$ and $2\theta_n$ are the phase shifts of the MC-GTE-*a* and the MC-GTE-*b*; L_1 and L_2 are distances from the MC-GTE-*a* and MC-GTE-*b* to the beam splitter, respectively.

For an *mn*-GTE interleaver, both the GTE and MI are interferometers. The phase shift of a single-cavity etalon for the GTE is δ while the phase shift for the MI is $\beta\cdot\triangle L$. When combining both interferometers to build a flattop interleaver, the phase shift of the single-cavity etalon has to be twice the phase shift due to the MI (i.e., $\delta = 2\beta\cdot\triangle L$), analogous to the *L* and 2*L* structures for a flattop digital filter design. By using the relations $\delta = 2\beta\cdot\triangle L$, we can obtain the intensity of the interleaver:

$$I = \left(1+\cos(2\triangle\psi-\delta)\right)/2. \tag{10}$$

2.1.3 Special features

There are two special features of an *mn*-GTE interleaver that we would like to emphasize:

1) The normalized half maximum intensity (i.e., ½ or 3dB) is always at $\delta = \pi/2+2p\pi$ (p is an integer), no matter what are the reflection coefficients chosen. In other words, all the spectral curves that result from different values of the reflection coefficients will intersect at half maximum intensity, i.e., ½ or 3dB. This can be easily proved with Eqs. (7) - (10).
2) The normalized intensity in the passband and that in the stopband of the interleaver are complementary. In a spectrum, the stopband corresponds to a wavelength band with a π phase shift relative to the passband. If we use $\delta' = \delta+\pi$ (for the stopband) to replace δ (for the passband) in Eq. (10), we can find the corresponding normalized intensity $I' = \left(1-\cos(2\triangle\psi-\delta)\right)/2$, which is obviously complementary with intensity *I*, because $I+I' = 1$. This is a very useful relationship as will be seen in the next subsection on the ripple and isolation performance.

2.2 Strategy for design optimization

From Eqs. (9) - (10), we can see that the interleaver spectrum is totally dependent on the two sets of reflection coefficients $r_0^a, r_1^a, ..., r_m^a$ and $r_0^b, r_1^b, ..., r_n^b$. Obviously, for the simple case of a 10-GTE interleaver, there is only one parameter r_1^b, and one can easily obtain the flattop spectrum. However, as the numbers of cavities increase in either arm, there are more parameters that need to be determined and optimized in order to obtain a desirable spectrum, i.e., flattop spectral response. In this section, we introduce a new optimization method, which has two steps – basic flattop conditions for an initial optimization point and ripple

#79720 - $15.00 USD Received 5 Feb 2007; revised 10 Apr 2007; accepted 17 Apr 2007; published 11 May 2007

equalization for final optimization. Examples of 11-GTE and 12-GTE interleavers will be used for illustration.

2.2.1 Initial optimization using basic flattop conditions

The flattop condition [16] for spectral response corresponds to a general condition (including reflection coefficients), where the transmission has a unit magnitude. By setting $\delta = 2p\pi$, the unit transmission is established around the central wavelength region, other than the center wavelength. From Eq. (10), the unit transmission requires

$$2\Delta\psi - \delta = 2p\pi. \tag{11}$$

Simplifying Eqs. (7-11), the general unit transmission equations for 10-GTE, 11-GTE and 21-GTE interleavers can be expressed as:

$$\begin{aligned} 2a_1 &= 1-\tan^2(\delta/2), \\ 2(a_1-b_1) &= (1-\tan^2(\delta/2))(1+a_1b_1\tan^2\delta), \\ 2\left[a_2(1+a_1)-b_1(1-a_1\tan^2\delta)\right] &= (1-\tan^2(\delta/2))\left[1+(a_2(1+a_1)b_1-a_1)\tan^2\delta\right]. \end{aligned} \tag{12}$$

From Eq. (12), by setting $\delta = 2p\pi$, one can obtain the flattop conditions for the 10-GTE, 11-GTE and 21-GTE interleavers as the following:

$$\begin{aligned} 2a_1 &= 1, \\ 2(a_1-b_1) &= 1, \\ 2(a_2(1+a_1)-b_1) &= 1. \end{aligned} \tag{13}$$

Accordingly, the flattop condition for an *mn*-GTE interleaver is

$$2\left[a_m(1+a_{m-1}(1+a_{m-2}\cdots))-b_n(1+b_{n-1}(1+b_{n-2}\cdots))\right]=1. \tag{14}$$

To illustrate how the basic flattop condition works, as an example, we present a 11-GTE interleaver which has two variable parameters r_1^a and r_1^b. Figure 3(a) shows the periodic spectra for different values of r_1^b, where r_1^a is determined by the flattop condition $2(a_1-b_1)=1$. It is clear that all the curves intersect at half maximum intensity ½, and the normalized intensity in the passband and that in the stopband of the interleaver are complementary. These are the two special features mentioned earlier.

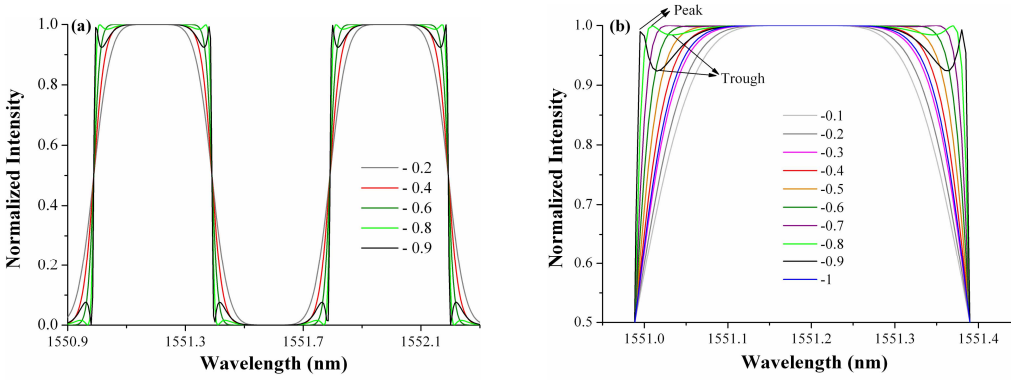

Fig. 3. (a). Periodic spectra of 11-GTE interleaver with different reflection coefficients and (b) detailed spectra of (a).

#79720 - $15.00 USD Received 5 Feb 2007; revised 10 Apr 2007; accepted 17 Apr 2007; published 11 May 2007

To clearly see how the reflection coefficients affect the spectral responses, Fig. 3(b) gives the spectra (only passband region) for different values of r_1^b from –0.1 to –1. It is very clear from Fig. 3(b) that there is a flattop region around the central wavelength region, which confirms the flattop condition. Note that the curve with $r_1^b = -1$ falls between the curve $r_1^b = -0.3$ and $r_1^b = -0.4$. This is because that $r_1^b = -1$ is a special case where the one-cavity GTE becomes a single regular reflector. So, it is equivalent to a 10-GTE interleaver. From the first equation in Eq. (13), one can easily obtain the optimal reflection coefficient for a 10-GTE interleaver, which is –1/3, i.e., –0.333 [13]. This is the reason why the curve falls between the curve $r_1^b = -0.3$ and $r_1^b = -0.4$.

It can also be seen that as the value of $|r_1^b|$ increases, one peak and one trough symmetrically appear on either side of the center wavelength; these extreme points move outwards and the trough gets deeper, resulting in a wider bandwidth but with a large ripple. The positions of the peak and the though determine the bandwidth, ripple, and isolation. The peaks correspond to the condition of unit transmission while the troughs correspond to the local minima. The position of the peak can be obtained by using the second equation in Eq. (12) and the flattop condition $2(a_1 - b_1) = 1$:

$$\tan^2 \frac{\delta_{peak}}{2} = 1 - 4a_1 b_1. \tag{15}$$

The position of the trough can be derived by differentiating the normalized intensity relative to the phase shift: $dI / d\delta = 0$. The results may be written as:

$$\sin^2 \delta_{trough} = \frac{1 - a_1 b_1 - a_1^2 - b_1^2}{(1 - a_1^2)(1 - b_1^2)}. \tag{16}$$

Both Eqs. (15) and (16) are quadratic equations. There are two roots for the peaks $\pm\delta_{peak}$, and two roots for the troughs $\pm\delta_{trough}$, which correspond to the positions of two peaks and two troughs on the left and the right of the center wavelength. Obviously, the positions of the peak and the trough depend on the two reflection coefficients r_1^a or r_1^b, as the flattop condition requires $2(a_1 - b_1) = 1$. By using Eqs. (15) and (16), we have plotted the positions of the peak and the through, and the ripple as functions of the reflection coefficient r_1^b (see Fig. 4), where r_1^a is chosen based on the flattop condition. Note that δ_{peak} and δ_{trough} are the optical phases and they may be used to represent the bandwidth. When δ is equal to 90°, the maximum (or ideal) bandwidth is reached. By inspecting Fig. 4, one can see the following points:

#79720 - $15.00 USD Received 5 Feb 2007; revised 10 Apr 2007; accepted 17 Apr 2007; published 11 May 2007

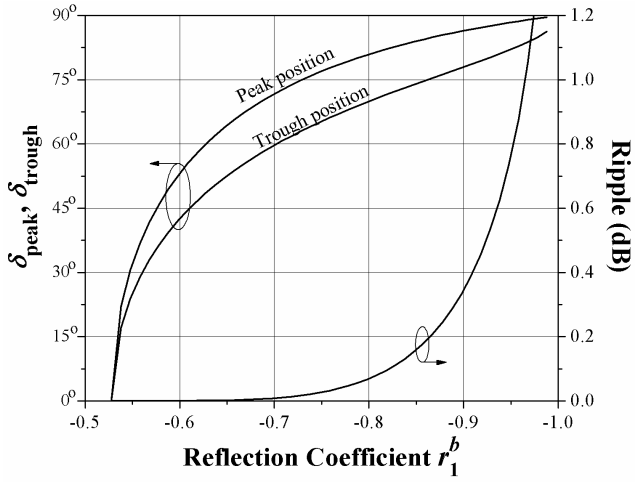

Fig. 4. Phases and ripples as functions of reflection coefficients.

1) The curves for the positions of the peak and the trough cross at $r_1^b = -0.53$. The value of r_1^b at the cross point can be precisely found from Eq. (15) and Eq. (16) by setting both equations to zero and imposing the flattop condition. It is interesting to see that both equations give the same reflection coefficients $r_1^b = -5 + 2\sqrt{5} \doteq -0.53$; this suggests that the two curves converge at $r_1^b = -0.53$.
2) The pure flattop region actually occurs at $|r_1^b| \le 0.53$, but from Fig. 4, one can see that the ripple can be extremely small at $|r_1^b| < 0.62$. When $|r_1^b| > 0.62$, the ripple increases with increase of $|r_1^b|$, but the phase δ_{peak} also increases, i.e., the passband bandwidth is enhanced.

2.2.2 Final optimization using ripple equalization

From the above discussion, we can see that the general condition works well when $|r_1^b| < 0.62$. In this subsection, we shall demonstrate that optimization may be completed by using the technique of ripple equalization when $|r_1^b| > 0.62$ for the 11-GTE interleaver. This method is also applied to optimize a 21-GTE interleaver in this subsection.

First, for a 11-GTE interleaver with two single-cavity etalons in an MI, in general, it is expected to have two resonant peaks and two troughs symmetrically distributed on either side of the center wavelength. This can be confirmed by the condition of unit transmission in Eq. (12). Simplifying the second equation in Eq. (12), one can obtain a quartic equation for the peak positions:

$$\tan^4(\delta/2) + B_1 \cdot \tan^2(\delta/2) + C_1 = 0, \tag{17}$$

where $B_1 = 2(a_1 - b_1) - 2 + 4a_1b_1$ and $C_1 = 1 - 2(a_1 - b_1)$. The quartic equation above may be reduced to a quadratic equation as

$$\tan^2\frac{\delta}{2} = \frac{-B_1 \pm \sqrt{B_1^2 - 4C_1}}{2}. \tag{18}$$

This equation has four roots, i.e, $\pm\delta_{peak1}$ and $\pm\delta_{peak2}$, corresponding to two peaks on either side. If the flattop condition is enforced, then $B_1 = 4a_1b_1$ and $C_1 = 0$, and Eq. (18) returns to

#79720 - $15.00 USD Received 5 Feb 2007; revised 10 Apr 2007; accepted 17 Apr 2007; published 11 May 2007

Eq. (15). Similarly, by differentiating the normalized intensity *I* relative to δ, one can find another quartic equation for the positions of the troughs:

$$A_2 \cdot \sin^4 \delta + B_2 \cdot \sin^2 \delta + C_2 = 0, \tag{19}$$

where $A_2 = (1-a_1^2)^2(1-b_1^2)^2$, $B_2 = 2a_1(a_1^2-1) - 2b_1(a_1^2-1) - a_1^2 - b_1^2 + 2$, and $C_2 = 2(a_1 - b_1) - 1$. The quartic equation may be reduced to a quadratic equation as

$$\sin^2 \delta = \frac{-B_2 \pm \sqrt{B_2^2 - 4C_2}}{2A_2}. \tag{20}$$

The above equation has four roots, i.e, $\pm\delta_{trough1}$ and $\pm\delta_{trough2}$, corresponding to the two troughs on either side. If the flattop condition is enforced, then Eq. (20) is reduced to Eq. (16).

Now, we are ready to optimize the 11-GTE interleaver for the cases of $|r_1^b| > 0.62$. Since there are two troughs, it is apparent that ripple equalization would be the best approach to optimize the optical performance of the interleaver by minimizing the ripple in the passband and maximizing the isolation in the stopband. For a given set of reflection coefficients, the two ripples can be straightforwardly found by substituting the solutions of Eq. (20) into Eq. (10). For any reflection coefficient r_1^b, the initial value of r_1^a can be calculated from the flattop condition. Then, the optimization can be obtained by slightly varying r_1^a with an offset until the two ripples are equal.

As an example, we have plotted the optimized spectra in Fig. 5. In Fig. 5(a), we set $r_1^b = -0.9$, and compare the two spectra, one (in red) obtained by using ripple equalization, and the other (in grey) without ripple equalization. Of course, the flattop condition has been applied to both cases. It is very clear that the ripple is greatly reduced with a negligible reduction of bandwidth. Figure 5(b) shows the effect of the reflection coefficients r_1^b on the spectra. One can see that as $|r_1^b|$ increases, both the optimized peaks (P and P') and the troughs (T and T') move outwards, and the magnitudes of the ripples increase. The effect of the reflection coefficient $|r_1^b|$ on the positions of the peaks and troughs are shown in Fig. 6, where the P's and T's have meanings as indicated in Fig. 5(b); the symbols with subscripts refer to cases where ripple equalization has applied; symbols without subscripts refer to cases that have the flattop condition only. One can clearly see that as $|r_1^b|$ increases, the phases of peaks and troughs increase; in other words, the bandwidth is improved.

#79720 - $15.00 USD Received 5 Feb 2007; revised 10 Apr 2007; accepted 17 Apr 2007; published 11 May 2007

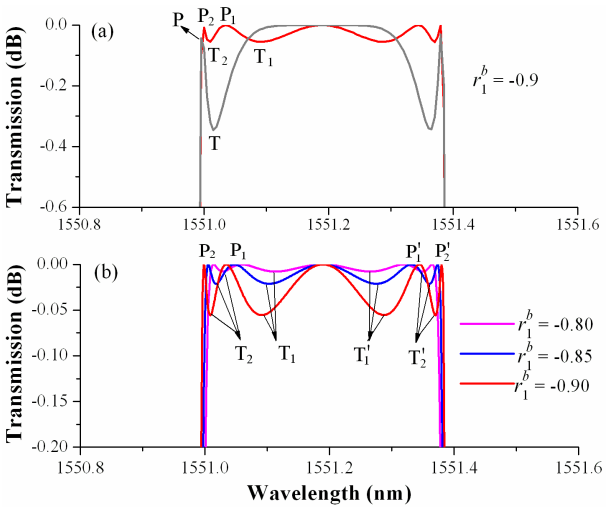

Fig. 5. Optimized spectra of 11-GTE interleaver: (a) comparison between optimized and non-optimized interleavers and (b) effects of different reflection coefficients.

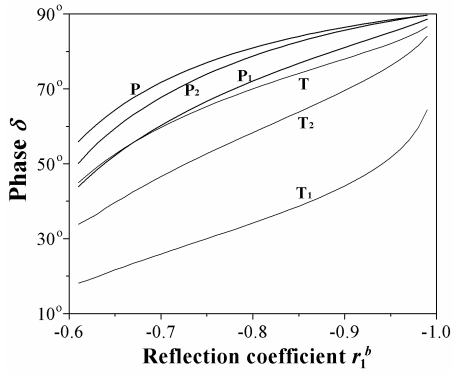

Fig. 6. Phase as a function of reflection coefficient.

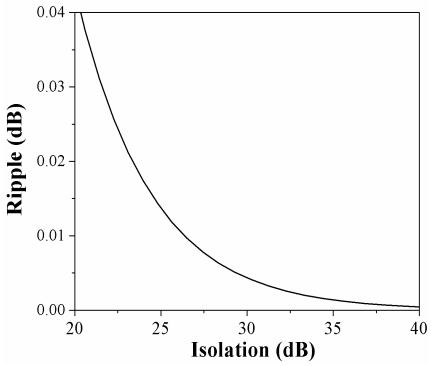

Fig. 7. Relation between ripple and isolation.

For interleavers, the ripple, bandwidth and isolation are the basic specifications. Assuming a lossless device, the maximum intensity at the center wavelength is unity. Based on this assumption, if the normalized intensity at the trough position is *P*, then the magnitude of the ripple is equal to $-10\log_{10} P$ dB. In industry, bandwidth is usually defined as the spectral width at a given power level. Here we define bandwidth as the spectral width at the power level *P* (i.e., normalized intensity at the trough position). Since bandwidth always varies with the free-spectral range (FSR), we use the bandwidth ratio, i.e., the ratio of the bandwidth to maximum bandwidth (which is equal to half of FSR) to evaluate the bandwidth so that it is independent of the channel spacing of the device. As to isolation, in industry, it is defined as the power difference between maximum insertion loss measured within a given passband window and the minimum insertion loss measured within the adjacent stopband window. Due to the complementary feature of the normalized intensities in the passband and in the stopband, the isolation can be evaluated from the ripple in the passband, based on the same bandwidth of passband and stopband. For example, if the normalized intensity at the trough position is *P*, the isolation can be expressed as $-10\log_{10}[(1-P)/P]$, and as stated above the ripple can be written as $-10\log_{10} P$. The relation of the ripple and the isolation is plotted in Fig. 7. This suggests that if such an interleaver has an extremely low ripple, it surely will have an extremely high isolation.

#79720 - $15.00 USD Received 5 Feb 2007; revised 10 Apr 2007; accepted 17 Apr 2007; published 11 May 2007

Based on the definitions above, Fig. 8 shows the bandwidth ratio and isolation as functions of the reflection coefficient r_1^b. Obviously, as $|r_1^b|$ increases, the bandwidth ratio increases, but the isolation decreases. In Fig. 9, we have plotted the optimized reflection coefficient r_1^a and ripple as functions of r_1^b for the range of $|r_1^b| > 0.62$ in two cases – with and without the technique of ripple equalization. The large reduction in ripple produced by optimization is very obvious. It can also be seen that beyond the flattop region (i.e., $|r_1^b| > 0.62$), with regard to the optimized reflection coefficient r_1^a, the difference between applying and not applying ripple equalization (denoted by "offset" in the figure) increases as $|r_1^b|$ increases.

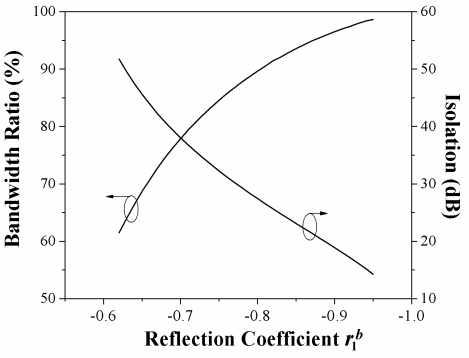

Fig. 8. Bandwidth ratio and isolation as functions of reflection coefficient. Ripple equalization has been used.

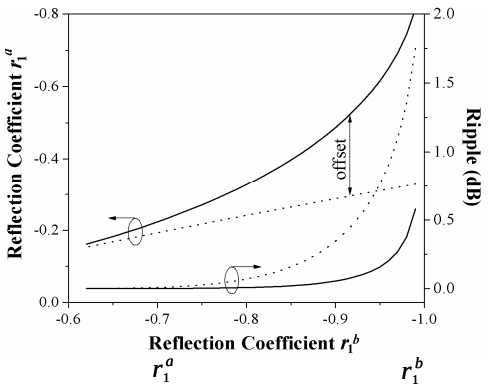

Fig. 9. Optimized and ripple as functions of for 11-GTE interleaver. Dotted lines: flattop condition used only. Solid lines: ripple equalization also applied.

In above discussion, we have seen that our optimization strategy works well for a 11-GTE interleaver. The proposed optimization strategy can also be applied to high-order GTE interleavers. As a demonstration, we show how the optimization strategy works for a 21-GTE interleaver to achieve enhanced performance.

For a 21-GTE interleaver, three peaks and three troughs are expected to be located on either side of the center wavelength. By simplifying the third equation in Eq. (12), we can obtain a polynomial equation for the positions of the peaks as

$$\tan^6(\delta/2) + E_1 \cdot \tan^4(\delta/2) + F_1 \tan^4(\delta/2) + G_1 = 0, \tag{21}$$

where $E_1 = 4x + z - 2$, $F_1 = 4y - 2z + 1$, and $G_1 = z$, with $x = b_1 a_1 (1 + a_1) - a_1$, $y = a_1 + b_1 a_1 (1 + a_1) - a_1$, and $z = 2a_2(1 + a_1) - 2b_1 - 1$. This equation has a degree of 6, which suggests that there will be six roots, corresponding to the six peaks. Equation (21) can be further reduced to a cubic equation, giving three different roots, corresponding to the three different pairs of peaks that distribute symmetrically relative to the center wavelength. Similarly, we can also obtain a polynomial equation for the positions of troughs as:

$$D_2 \sin^6 \delta + E_2 \sin^4 \delta + F_2 \sin^2 \delta + G_2 = 0, \tag{22}$$

where $D_2 = h_1 h_2 h_3^2$, $E_2 = 2a_1 h_1 k_1 + (1 + 2b_1) h_2 h_3^2 - k_1 (h_1 + h_1 h_3^2)$, $F_2 = 2a_1 (h_1 + k_1) - (1 + 2b_1)(h_1 + h_1 h_3^2) - k_1$, and $G_2 = 2a_1 h_3 - 2b_1 - 1$, with $h_{1,2} = a_{1,2}^2 - 1$, $k_1 = b_1^2 - 1$, and $h_3 = a_1 + 1$. Once again, Eq. (22) is a polynomial equation with a degree of 6, which can be reduced to a cubic equation that gives

#79720 - $15.00 USD Received 5 Feb 2007; revised 10 Apr 2007; accepted 17 Apr 2007; published 11 May 2007

the positions of the three different pairs of troughs located symmetrically relative to the center wavelength.

By using both the flattop condition and the technique of ripple equalization, we can optimize the spectrum for a 21-GTE interleaver. For illustration, we have plotted the optimized spectra for three different reflection coefficients $|r_1^b|$ as shown in Fig. 10. One can see that there are three pairs of peaks and three pairs of troughs as predicted and the ripples are all equalized for optimal performance. It can also be seen that low ripple and high isolation can be obtained by choosing small $|r_1^b|$, while a large bandwidth can be obtained by using large $|r_1^b|$. Note that for a given reflection coefficient $|r_1^b|$, there is only one set of optimized values for $|r_1^a|$ and $|r_2^a|$, which would have all three ripples equalized. This means that for a particular ripple, or bandwidth specification, the reflection coefficients are uniquely determined. The relations of the three optimized reflection coefficients are displayed in Fig. 11. It shows that the optimized $|r_1^a|$ and $|r_2^a|$ increase with the increase of $|r_1^b|$, and that the reflectivity (i.e., $|r_1^a|^2$) of M_1^a (the reflector closest to the rear 100% reflector) is much higher than that (i.e., $|r_2^a|^2$) of M_2^a. This is due to the recursive feature of a GTE device, which will be seen in the next section about chromatic dispersion compensation.

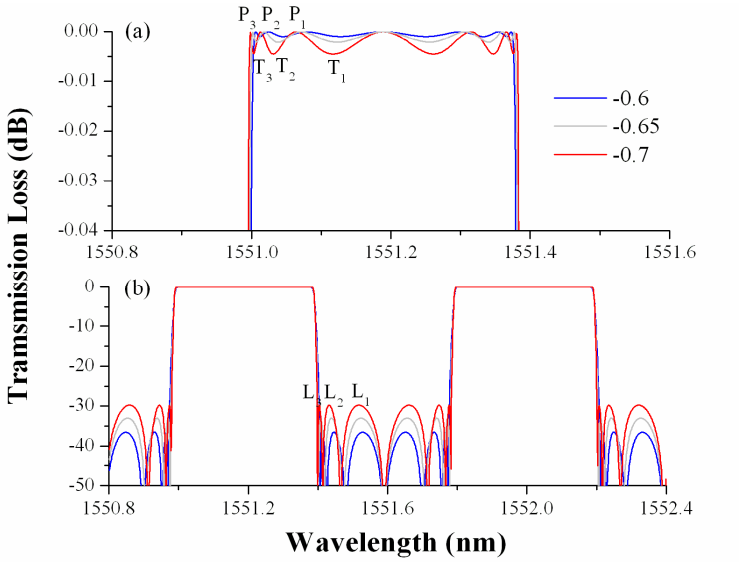

Fig. 10. Optimized spectra of 21-GTE interleaver with different reflection coefficient r_1^b: (a) detailed passband and (b) one FSR.

#79720 - $15.00 USD Received 5 Feb 2007; revised 10 Apr 2007; accepted 17 Apr 2007; published 11 May 2007

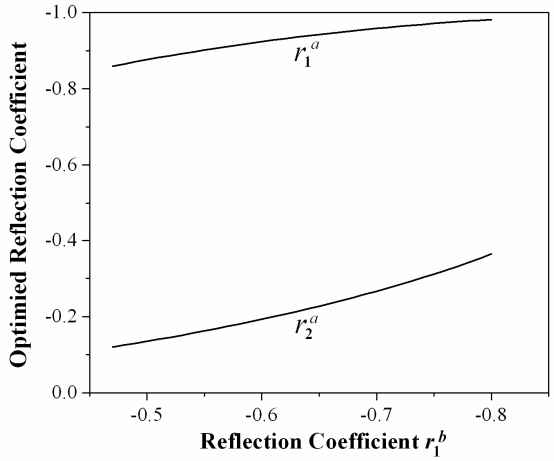

Fig. 11. Optimized reflection coefficients r_1^a and r_2^a and ripple as functions of reflection coefficient r_1^b for a 21-GTE interleaver.

In the above discussion, we presented the optimization method for a 11-GTE and a 21-GTE interleaver. The motivation of employing more cavities is to enhance the optical performance. Note that each optimized set of reflection coefficients will give one set of optimized bandwidth ratio, ripple or isolation as shown in Fig. 8. To compare the optical performance of different configurations, we show the bandwidth ratio as a function of isolation for a 10-GTE, a 11-GTE, and a 21-GTE interleaver in Fig. 12. The figure clearly shows that assuming a fixed isolation, the bandwidth ratio can be improved by increasing the number of cavities, and vice versa. In Table 1, we give a list of bandwidth ratios at three fixed isolations for different configurations. For example, if the isolation is fixed at 28 dB, then the ripple is 0.0069 dB, and the bandwidth ratios that can be reached by optimization are 62.6%, 89.1% and 96.8% for the10-GTE, 11-GTE and 21-GTE interleaver, respectively. As stated earlier, the stopband bandwidth for isolation is equal to the passband bandwidth, which means that the isolation of 28 dB is based on the stopband bandwidth ratio of 89.1% for a 11-GTE interleaver; on the other hand, the bandwidth ratio is calculated based on the ripple level, which means that the passband bandwidth ratio is 89.1% at a power level of 0.0069 dB down for a 11-GTE interleaver.

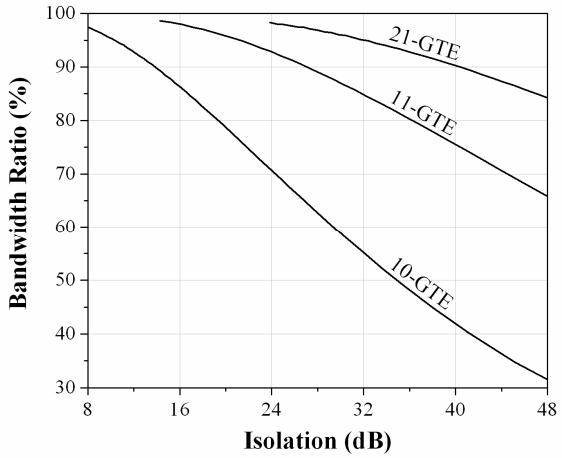

Fig. 12. Bandwidth ratio as a function of isolation for GTE interleavers with different configurations.

#79720 - $15.00 USD Received 5 Feb 2007; revised 10 Apr 2007; accepted 17 Apr 2007; published 11 May 2007

Table 1 Bandwidth ratio for different configurations

ISO (dB)	Ripple (dB)	Bandwidth ratio		
		10-GTE	11-GTE	21-GTE
24	0.0173	70.6%	92.8%	98.0%
28	0.0069	62.6%	89.1%	96.8%
32	0.0027	55.1%	84.8%	95.0%

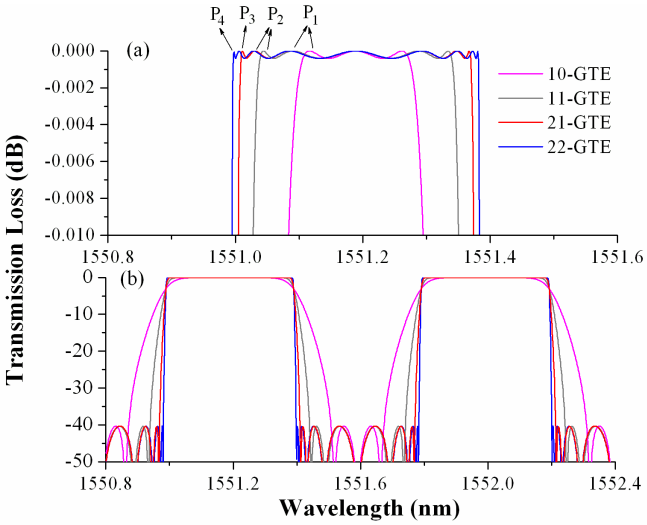

Fig. 13. Optimized spectra for interleavers with different configurations: (a) detailed passband and (b) one FSR.

From both Fig. 12 and Table 1, we can see that the optical performance is greatly enhanced by increasing the number of cavities. As a demonstration, in Fig. 13, we have plotted the spectra for four different configurations based on the same ripple level of 0.0004 dB, corresponding to the isolation of 40 dB. It is very clear that the spectra are well optimized with the proposed optimization strategy. As the number of cavities increases, the number of resonant peaks increases; this leads to an enhancement of the bandwidth. Note that the number of peaks or troughs is equal to the sum of the cavities $m+n$. For example, a 22-GTE interleaver has four peaks and four troughs on either side of the center wavelength.

3. Chromatic dispersion compensation for flattop interleaver

Chromatic dispersion is another key specification for interleavers. It is an unavoidable issue for IIR-based (e.g., etalon-based) interleavers. It greatly degrades the performance of the optical network systems. In order to achieve a low-dispersion interleaver, chromatic dispersion compensation for flattop interleaver is necessary. In this paper, we propose to use an additional lossless MC-GTE to compensate for the dispersion introduced by the proposed interleaver. Since our proposed interleaver is also based on the MC-GTE, in order to analyze the dispersion property of MC-GTE based devices, i.e., the dispersion compensator and the interleaver, firstly, we need to find the general analytical expression of the group delay and dispersion for the MC-GTE, and investigate the chromatic dispersion of the proposed interleaver. Then we will present the principle of the dispersion compensator, followed by design optimization for dispersion compensations.

3.1 Group delay and chromatic dispersion for MC-GTE

From our earlier discussion in section 2.1.1, we obtained the optical phase for an MC-GTE with any number of cavities as given in Eq. (4). It is a recursive function, with the initial phase

#79720 - $15.00 USD Received 5 Feb 2007; revised 10 Apr 2007; accepted 17 Apr 2007; published 11 May 2007

$\phi_1 = -\tan^{-1}(a_1 \tan\delta)$. Accordingly, the group delays for 1-, 2-, 3-, and *n*-cavity GTE can be derived as:

$$\begin{aligned} GD_1 &= 2\tau c_1 \quad \text{(one cavity)}, \\ GD_2 &= 2\tau c_2 (1+c_1) \quad \text{(two cavities)}, \\ GD_3 &= 2\tau c_3 (1+c_2 (1+c_1)) \quad \text{(three cavities)}, \\ GD_n &= 2\tau c_n + c_n GD_{n-1} \quad (n \text{ cavities}), \end{aligned} \tag{23}$$

with

$$c_n = \frac{a_n}{1+(a_n-1)^2 \sin^2(\delta-\phi_{n-1})}, \tag{24}$$

where $\tau = nd/c$ is a unit time delay of a single cavity. Based on Eqs. (23) – (24), the corresponding chromatic dispersions can be written as:

$$\begin{aligned} CD_1 &= 2h\tau g_1 \quad \text{(one cavity)}, \\ CD_2 &= 2h\tau \left[g_2 (1+c_1)^2 + g_1 c_2 \right] \quad \text{(two cavities)}, \\ CD_3 &= 2h\tau \left[g_3 (1+c_2(1+c_1))^2 + c_3 \left(g_2 (1+c_1)^2 + g_1 c_2 \right) \right] \quad \text{(three cavities)}, \\ CD_n &= 2h\tau \left[g_n \left(\frac{GD_n}{2\tau c_n} \right)^2 + c_n \left(\frac{CD_{n-1}}{2h\tau} \right) \right] \quad (n \text{ cavities}), \end{aligned} \tag{25}$$

with

$$h = 2\pi nd/\lambda^2, \tag{26}$$

$$g_n = \frac{(a_n^2-1)a_n \sin 2(\delta-\phi_{n-1})}{\left[1+(a_n^2-1)^2 \sin^2(\delta-\phi_{n-1})\right]^2}. \tag{27}$$

It is very interesting to observe the following points about group delay and chromatic dispersion of an MC-GTE from above equations:

1. From Eqs. (23) and (24), the group delay of a single-cavity GTE has an Airy function, similar to the transmitted intensity of a Fabry-Perot etalon [30]. The group delay has a periodic response with a maximum value of $2\tau_1 a_1$ and a minimum value of $2\tau_1 a_1 / [1+(a_1^2-1)^2]$.
2. From Eq. (25), one can see that the chromatic dispersion is proportional to $(nd)^2$. This suggests that for a GTE, if FSR is halved, the chromatic dispersion will be increased by four times as FSR is inversely proportional to $(nd)^2$.
3. Like the resultant reflection coefficient and the resultant phase, the group delay and chromatic dispersion of an *n*-cavity GTE are all recursive functions.

Now, from Eqs. (6) and (7), one can find that the phase of any *mn*-GTE interleaver is the sum of the phases (i.e., $\phi_m + \theta_n$) of the two MC-GTEs, so the group delay and chromatic dispersion of any *mn*-GTE interleaver are the sum of those of the two MC-GTEs, each of which can be obtained from Eqs. (23) and (25). In Figs. 14(a) and 14(b), we show the responses of group delays and dispersions for a 10-GTE, and a 21-GTE interleaver, with the same reflection coefficients used in Fig. 13. Obviously, there are dispersion and dispersion slope in passband, and with increasing the number of cavities, group delay, dispersion and dispersion slope increase.

#79720 - $15.00 USD Received 5 Feb 2007; revised 10 Apr 2007; accepted 17 Apr 2007; published 11 May 2007

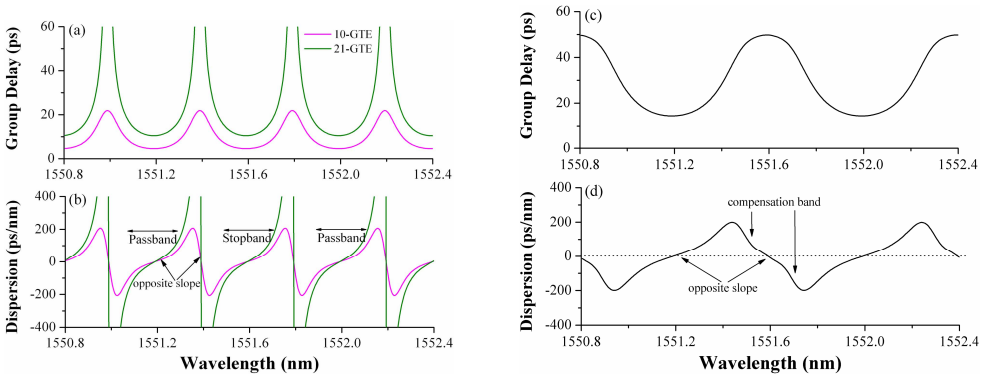

Fig. 14. (a). Group delay and (b) dispersion responses for 10-GTE and 21-GTE interleaver; (c) group delay and (d) dispersion responses for typical MC-GTE dispersion compensator.

3.2 Principle of chromatic dispersion compensator and design optimization

In principle, to completely compensate the chromatic dispersion (*CD*) and dispersion slope (*DS*) of the proposed interleaver in passband, the dispersion compensator must have exactly the same dispersion and dispersion slope as that of interleaver, but with *opposite* sign, i.e., -*CD* and -*DS*, respectively. From Fig. 14(b), one may notice that there are positive and negative sloping sections in the pink curve (though the two slopes are not equal) for a 10-GTE interleaver, which suggests that MC-GTE may have similar dispersion curve shape as the phase of *mn*-GTE inteleaver is the sum of the phases of the two MC-GTEs. This is why MC-GTE may be used as dispersion compensator. Figures 14(c) and 14(d) show the group delay and dispersion responses for a typical MC-GTE dispersion compensator; the compensation band in Fig. 14(d) with negative slope could be used to compensate for the dispersion with positive slope in the passband in Fig. 14(b). Note that the FSR of an *mn*-GTE interleaver for spectrum in Fig. 13 is twice of that for group delay and dispersion in Figs. 14(a) and 14(b) due to the setting $\delta = 2\beta \cdot \Delta L$ (see Section 2.1.2). Therefore, the FSR of the MC-GTE for dispersion compensators has to be twice of that for building inteleavers, as can be seen in Figs. 14(d) and 14(b). Note that when cascading the compensator with the interleaver, it is necessary to align the center wavelength by shifting half of the FSR as the compensation band of the compensator is centred in the stopband of the interleaver. By suitably choosing the reflection coefficients of the MC-GTE, the shape of the dispersion curve may be tailored to cancel the dispersion and dispersion slope introduced by interleavers within a certain passband.

In the following we demonstrate the compensation of the dispersion of a 21-GTE interleaver by using an MC-GTE. As seen in Eq. (23) and Eq. (25), the group delay and chromatic dispersion of an *n*-cavity GTE are all recursive functions. This suggests that the performance of the dispersion compensation can be enhanced by using more cavities, because more parameters, i.e., reflection coefficients are available to tailor the shape of the dispersion curve. It is the unique recursive relations that allow MC-GTEs to be powerful devices for dispersion compensation, as can be seen in Fig. 15.

Figure 15(a) shows the dispersions of a 21-GTE interleaver compensated by 2-, 3- and 4-cavity GTE compensators. The black solid line is the dispersion of the 21-GTE interleaver without compensation, the dotted lines correspond to the dispersions of compensators with 2, 3 and 4 cavities, and the colored solid lines give the resultant dispersions of the 21-GTE interleaver after being compensated by 2-, 3-, and 4-cavity GTEs. One can clearly see in Fig. 15(a) that the colored solid lines have a quasi-flat region in the passband, which confirms that low chromatic dispersions are achieved. The details inside the quasi-flat regions are shown in Fig. 15(b). One can see that there is a dispersion ripple of ±2 ps/nm. Similar to the

#79720 - $15.00 USD Received 5 Feb 2007; revised 10 Apr 2007; accepted 17 Apr 2007; published 11 May 2007

optimization strategy for spectrum, i.e., ripple equalization, we use the approach of the dispersion ripple equalization to optimize the dispersion compensators. For example, for a 4-cavity compensator, there are two troughs (T_1 and T_2), and two peaks (P_1 and P_2) on either side of the center wavelength. The absolute values of the dispersions at the four points are equalized by suitably choosing the reflection coefficients of the four reflectors for dispersion optimization.

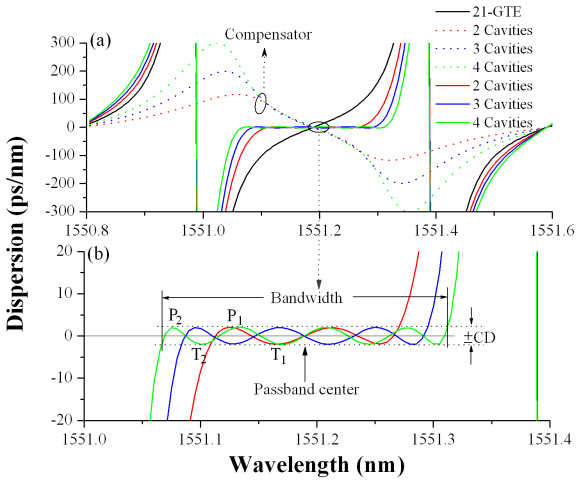

Fig. 15. (a). Resultant dispersion of 21-GTE interleaver compensated by MC-GTEs with different number of cavities. (b). Details of the quasi-flat dispersion region.

In general, for an interleaver, chromatic dispersion is defined as the maximum dispersion within a given passband bandwidth. So, to evaluate the dispersion performance of our dispersion-compensated interleaver, we use dispersion *CD*, bandwidth [see Fig. 15(b)] and bandwidth ratio. Here the dispersion ripple is actually the dispersion *CD*; the bandwidth is the width within which the maximum dispersion is *CD*; the bandwidth ratio is the ratio of bandwidth to half FSR as defined earlier. Note that the number of troughs and peaks is equal to the number of cavities. Obviously, based on the same dispersion ripple, the bandwidth is clearly enhanced by increasing the number of cavities.

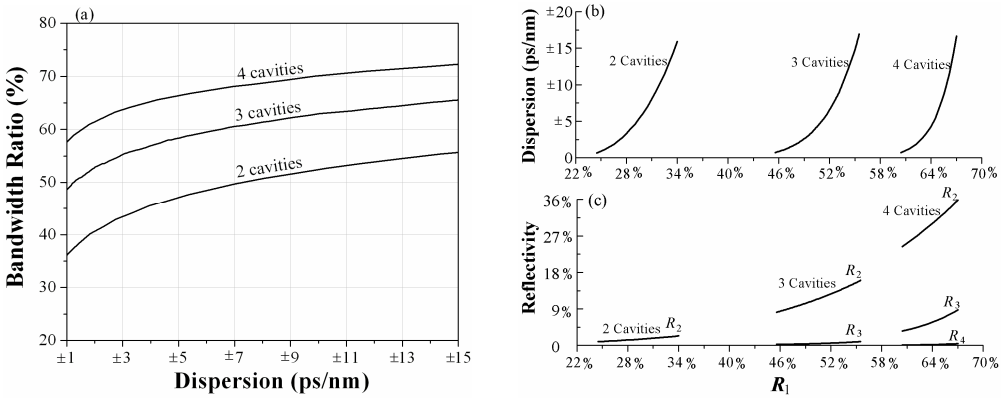

Fig. 16. Interleavers compensated by MC-GTEs with different number of cavities. (a) Bandwidth ratio as a function of dispersion; (b) Dispersion and (c) optimized reflectivities as functions of reflectivity R_1.

To compare the dispersion performance of 21-GTE interleavers compensated by MC-GTEs with different number of cavities, we have plotted the bandwidth ratio as a function of

#79720 - $15.00 USD Received 5 Feb 2007; revised 10 Apr 2007; accepted 17 Apr 2007; published 11 May 2007

CD in Fig. 16(a). It is clear that for the same *CD*, the bandwidth ratio can be greatly enhanced by adding more cavities. For example, within ±5 ps/nm of dispersion, the bandwidth ratio can reach 47%, 58.6%, and 66.6% for 2, 3 and 4 cavities, respectively. High bandwidth ratio can be achieved by relaxing the specification of the dispersion *CD*. For example, within ±10 ps/nm of dispersion, the bandwidth ratio can reach 52.3%, 62.7%, and 70% for 2, 3 and 4 cavities, respectively.

To see how the reflection coefficients can change the dispersion for different number of cavities, we have plotted the dispersion as a function of reflectivity R_1 in Fig. 16(b), and the optimized reflectivities are shown in Fig. 16(c). From Fig. 16(b), one can see that for the same dispersion the reflectivity R_1 increases with increasing number of cavities; low dispersion can be obtained by using small values of R_1. From Fig. 16(c), one can see that all the optimized reflectivities, R_2, R_3, and R_4, increase with increase of R_1, and the values of reflectivities follow the order of $R_1 >> R_2 >> R_3 >> R_4$, which can be attributed to the unique recursive relations of MC-GTEs.

4. Conclusion

We have thoroughly studied MC-GTE interleavers, including design optimization of spectral response and chromatic dispersion compensation to achieve flattop low-dispersion interleavers. For spectral response, flattop response is desirable and essential. The optimization strategy that we have proposed for flattop spectrum includes using the flattop conditions and ripple equalization. The flattop spectrum can be realized by suitably choosing the reflection coefficients based on flattop conditions. However, this method works well only when the reflectivities are small. As the reflectivities increase, the ripples degrade the performance. In such cases, the ripple equalization can be used to optimize the interleaver to achieve minimum ripples within wider passband bandwidth. Special examples of 11-GTE and 21-GTE interleavers are given to illustrate how the reflection coefficients can control the flattop response, the bandwidth, the isolation, and the ripple. Note that for an *mn*-GTE interleaver, the ripple and the isolation are interdependent because the intensity in the passband and that in the stopband of the interleaver are complementary. We also found that the number of peaks (or troughs) is equal to the sum of cavities ($m+n$) of an *mn*-GTE interleaver. When the number of cavities increases, the number of peaks increases, and the spectrum becomes wider, giving rise to an enhanced spectral performance.

For any *mn*-GTE interleaver, the chromatic dispersion is a challenging problem. We have thoroughly analyzed the dispersion and dispersion compensation of an *mn*-GTE interleaver by using an MC-GTE as a dispersion compensator. We have derived the expressions for the group delay and chromatic dispersion for *mn*-GTE interleavers. Dispersion ripple equalization is a strategy we have proposed and used to optimize the dispersion compensator. We have discussed the dispersion performance using MC-GTEs with different number of cavities. The results show that the dispersion performance can be tailored with the reflection coefficients of the MC-GTE; the dispersion and bandwidth can be enhanced by increasing the number of cavities of the MC-GTE. Note that the analytical expressions for the reflection coefficients, phase shifts, group delays, and chromatic dispersions are all recursive. The rule of thumb to choose the reflectivitites for an MC-GTE is $R_1 >> R_2 >> R_3 >> R_4$.

Acknowledgment

This work is supported by the Natural Sciences and Engineering Research Council of Canada (NSERC).

#79720 - $15.00 USD Received 5 Feb 2007; revised 10 Apr 2007; accepted 17 Apr 2007; published 11 May 2007